



## Glycine-Assisted Sol-Gel Combustion Synthesis and Characterization of Aluminum-Doped $\text{LiNiVO}_4$ for Use in Lithium-Ion Batteries

A. Sivashanmugam,<sup>a</sup> R. Thirunakaran,<sup>a</sup> Meijing Zou,<sup>b</sup> Masaki Yoshio,<sup>b,\*</sup> Jun-ichi Yamaki,<sup>c,\*</sup> and S. Gopukumar<sup>a,z</sup>

<sup>a</sup>Central Electrochemical Research Institute, Karaikudi 630 006, Tamil Nadu, India

<sup>b</sup>Department of Applied Chemistry, Saga University, Saga 840-8502, Japan

<sup>c</sup>Institute of Advanced Materials Chemistry and Engineering, Kyushu University, Kasuga Koen 6-1, Kasuga 816-8580, Japan

Phase-pure inverse spinel  $\text{LiNiVO}_4$  and  $\text{LiAl}_x\text{Ni}_{1-x}\text{VO}_4$  have been synthesized with good surface morphology by a sol-gel method using glycine as a chelating agent. The product was characterized by thermogravimetric and differential thermal analysis, X-ray diffraction, Fourier transform infrared spectroscopy, scanning electron microscopy, and galvanostatic cycling studies. Surface morphology examinations of the undoped  $\text{LiNiVO}_4$  particles showed micrometer-sized, cube-shaped grains, while that of aluminum-doped particles showed uniform spherical particles. As compared to the solid-state synthesis route, the sol-gel combustion process greatly reduces the temperature ( $250^\circ\text{C}$ ) for preparing  $\text{LiNiVO}_4$  and  $\text{LiAl}_x\text{Ni}_{1-x}\text{VO}_4$ . Subsequent calcination between  $650$  and  $850^\circ\text{C}$  significantly enhances the crystallinity of the synthesized  $\text{LiNiVO}_4$  and  $\text{LiAl}_x\text{Ni}_{1-x}\text{VO}_4$  powder. The discharge capacity and cycling performance of the  $\text{LiAl}_{0.1}\text{Ni}_{0.99}\text{VO}_4$  was found to be superior at a calcination temperature of  $250^\circ\text{C}$ .

© 2006 The Electrochemical Society. [DOI: 10.1149/1.2162454] All rights reserved.

Manuscript submitted August 31, 2005; revised manuscript received November 10, 2005.

Available electronically January 24, 2006.

Attempts to synthesize  $\text{LiNiVO}_4$  were made as early in 1961 by Bernier et al.<sup>1</sup> However, cathodic properties of the  $\text{LiNiVO}_4$  inverse spinel were first investigated by Fey et al. in 1994.<sup>2</sup>  $\text{LiNiVO}_4$  rates better than layered cathode materials such as  $\text{LiCoO}_2$ ,  $\text{LiNiO}_2$ , etc., in terms of toxicity, cost, and cell voltage ( $4.8\text{ V}$ ).<sup>3-8</sup> High-voltage cathodes ( $4.8\text{ V}$ ) such as  $\text{LiMnVO}_4$ ,  $\text{LiNiVO}_4$ , and  $\text{LiCoVO}_4$  have been synthesized as an important class of materials for use in lithium batteries. Further, these oxides have also been doped with either Co, Mn, etc. in order to realize superior electrochemical properties.

Sol-gel chemistry offers the advantage of synthesizing materials of uniform particle size and morphology at low temperatures and often materials that have attractive electrochemical activity. This contrasts with the solid-state-fusion method, which is time-consuming and energy-intensive, and hence, economically unwise.<sup>9</sup> Low-temperature synthesis of  $\text{LiNiVO}_4$  has been reported by Prabaharan et al.<sup>10</sup> from nitrate precursors using glycine as a fuel. The product formation was observed at  $320^\circ\text{C}$  with glycine at twice the molar fraction of the total stoichiometry of the starting materials. In contrast, we present in this paper our basic studies on the physical and electrochemical characterization of  $\text{LiNiVO}_4$  and  $\text{LiAl}_x\text{Ni}_{1-x}\text{VO}_4$ , synthesized using a novel glycine-assisted sol-gel combustion method where the product formation is achieved at  $250^\circ\text{C}$  at a lower (1:1) stoichiometry of glycine to the total metal ions.

### Experimental

A typical flow chart of the preparative process used in this work is presented in Fig. 1. Stoichiometric amounts of nitrate precursors (lithium, nickel, with or without aluminum) and ammonium metavanadate were stirred with glycine in deionized water for about 12 h. The amount of glycine was such that the molar ratio of the chelating agent to the total metal ions was maintained at 1:1. The pH of the mixture was maintained between 5 and 6. A foamy gel of the precursor of either  $\text{LiNiVO}_4$  or  $\text{LiAl}_x\text{Ni}_{1-x}\text{VO}_4$  obtained was dried in a vacuum oven at  $110^\circ\text{C}$  overnight. Thermogravimetric and differential thermal analyses of the precursor were carried out using a PL Thermal Sciences instrument model STA 1500. The experiments

were performed in air at a heating ramp of  $20^\circ\text{C}/\text{min}$  with typically 50-mg samples. The dried precursor powder was finely ground and calcined at  $250$ ,  $450$ ,  $650$ , and  $850^\circ\text{C}$  for 4 h in alumina crucibles. The calcined materials were subjected to X-ray diffraction (XRD), scanning electron microscopy (SEM), Fourier transform infrared (FTIR) studies. Powder XRD studies were performed on a Jeol JDX-8030 X-ray diffractometer with nickel-filtered  $\text{Cu K}\alpha$  radiation between scattering angles of  $10$  and  $70^\circ$ . FTIR spectra of the vanadate samples were recorded on a Perkin-Elmer Paragon-500 FTIR

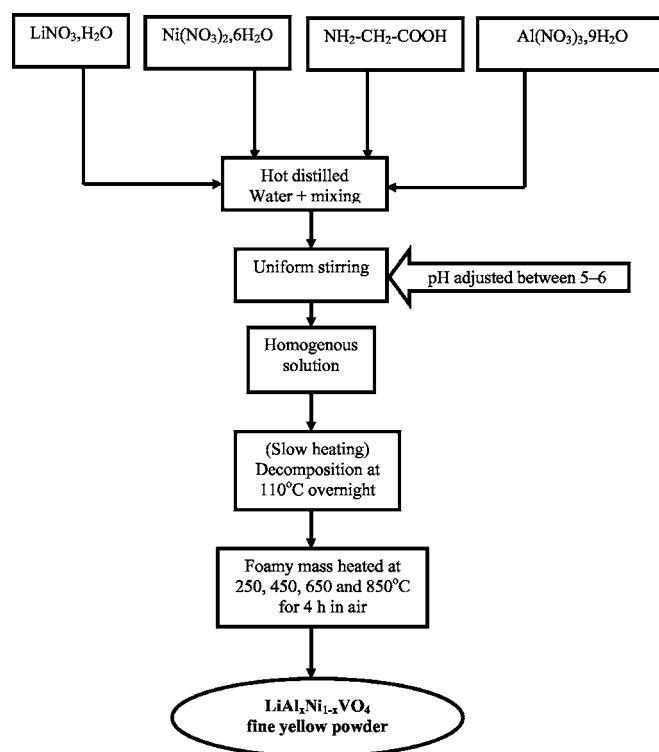


Figure 1. Flow chart for the synthesis of  $\text{LiNiVO}_4$  by a sol-gel combustion method using glycine as a chelating agent.

\* Electrochemical Society Active Member.

<sup>z</sup> E-mail: deepika\_41@rediffmail.com

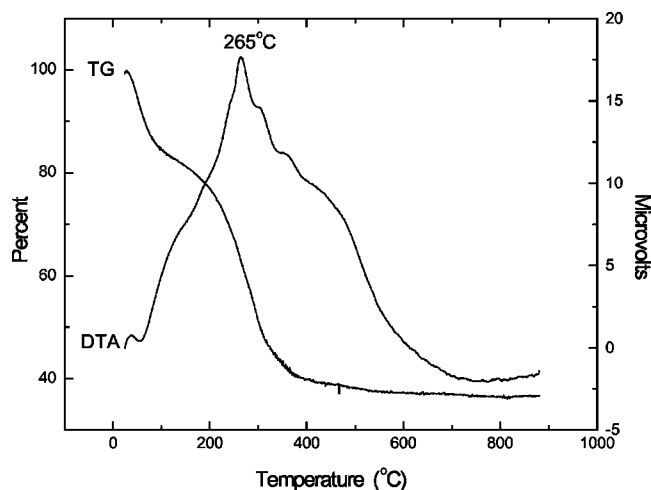


Figure 2. TG and DTA curves of  $\text{LiNiVO}_4$  precursor.

spectrophotometer. Morphological features of the products were examined in a Hitachi S-3000 H scanning electron microscope. Standard 2016 coin cells were assembled using lithium metal as anode, a Celgard 2400 separator, and 1 M solution of  $\text{LiPF}_6$  in a 50:50 (v/v) mixture of ethylene carbonate and diethyl carbonate. Cathodes were 1.8-cm-diam disks spread-coated with an 80:10:10 slurry of the cathode active powder, graphite, and polyvinylidene fluoride in *N*-methyl-2-pyrrolidone. Cathode active material loadings in the samples varied from 0.087 to 0.098 g. Charge-discharge studies were performed using an in-house charging facility between 3 and 5 V at 0.1 C rate.

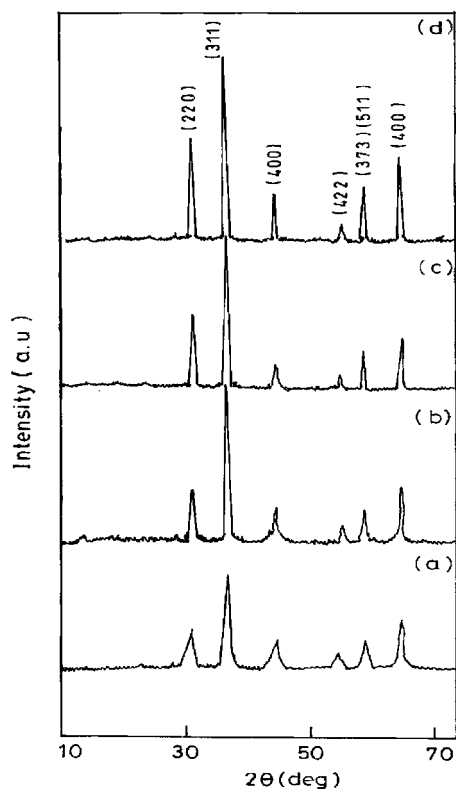


Figure 3. XRD patterns of the sol-gel-derived  $\text{LiNiVO}_4$  powders calcined at different temperatures: (a) 250, (b) 450, (c) 650, and (d) 850°C.

## Results and Discussion

**Thermal studies.**—Figure 2 shows the thermogravimetric (TG)/differential thermal analysis (DTA) characteristics of the  $\text{LiNiVO}_4$  precursor. The TG curve shows two rapid weight loss regions, sandwiching a slow weight loss region. The first rapid weight loss between room temperature and 100°C, accounting for a weight loss of 15%, can be attributed to the loss of superficial water. The second weight loss of 10% extending up to 200°C is relatively slow. Subsequently, a third weight loss region, which accounts for as much as 35%, is observed between 200 and 400°C. Major decomposition reactions of the reactants to yield the product occur in the second and third regions. No significant changes occur beyond 400°C, which indicates the completion of thermal events. The products form at temperatures represented by the second and third regions, supported by large exothermic peaks centered at around 265°C in the DTA curve. This inference is vindicated by the well-defined fingerprint XRD pattern of  $\text{LiNiVO}_4$  (Fig. 3), obtained by the calcination of the precursor at 250°C. Combustion synthesis with chelated precursors can be initiated at low temperatures; however, the local temperatures in the system can rise to more than 1000°C. The short duration and the high local temperatures facilitate bond formation and crystallization processes. Thus, thermal analysis data indicate the formation of  $\text{LiNiVO}_4$  at temperatures around 250°C.

Figure 4 shows the TG/DTA curves for  $\text{LiAl}_x\text{Ni}_{1-x}\text{VO}_4$  powders with different Al doping. Two exothermic peaks are seen in all the samples between 225 and 400°C, augmented with two weight-loss (45%) zones at around 100 and 250°C, attributed to the removal of water and the formation of the vanadate. A majority of the formation reactions ceases around 300°C, and beyond that no significant reactions take place with low Al doping levels. In the case of samples with higher Al contents, a weak exothermic event is witnessed at around 500°C, corresponding to a weight loss of ~10%. This may be attributed to the decomposition of aluminum nitrates.

**X-ray diffraction.**—The phase purity and homogeneity of  $\text{LiNiVO}_4$  is a necessary criterion for cathode activity in lithium-ion batteries. Figure 3 shows the XRD patterns of  $\text{LiNiVO}_4$  calcined at different temperatures, viz., 250, 450, 650, and 850°C. All the peaks match those of JCPDS card no. 38-1395, confirming the formation of single-phase inverse spinel structured compound without any impurity, even with the samples calcined at 250°C. This observation is in contrast to that of Fey et al.,<sup>2</sup> who suggested that a temperature of at least 700°C was necessary to obtain satisfactory crystallinity in  $\text{LiNiVO}_4$  powder by the conventional solid-state reaction process. Furthermore,  $\text{LiNiVO}_4$  prepared by the solid-state fusion method involves long reaction times. Additionally, carbonate and nitrate precursors employed in the solid-state fusion method add  $\text{VO}_3$  and NiO impurities, as has been observed by several researchers.<sup>3</sup> However, in the present method, product formation takes place at 250°C. It can be seen from Fig. 3 that the intensity of the XRD pattern increases with increasing calcination temperature. The high-intensity reflections observed with  $\text{LiNiVO}_4$  samples calcined at 850°C indicate a high degree of crystallinity for these samples. The XRD fingerprints of  $\text{LiNiVO}_4$  possess striking similarity with those of  $\text{LiCuVO}_4$ .<sup>11,12</sup> Nevertheless, the XRD pattern of  $\text{LiNiVO}_4$  calcined at 250 and 450°C show fairly weak reflections, indicating the amorphous nature of the compounds. Additionally, the positions of the tetrahedral and octahedral  $[\text{MO}_6]$  units in the structure were corroborated by FTIR analysis.

Figure 5 depicts the XRD patterns of  $\text{LiAl}_x\text{Ni}_{1-x}\text{VO}_4$  at different Al-doping levels, viz., 0.05, 0.1, 0.25, and 0.5 calcined at 850°C. The peak signatures of the pattern are in agreement with that of inverse spinel (JCPDS card no. 38-1395). The presence of an additional peak in the (111) plane is ascribed to the incorporation of aluminum and is probably due to the tendency toward the structural transformation from truly inverse spinel-to-spinel structure. The high degree reflection of plane (311) indicates the highly crystalline state of the particles.

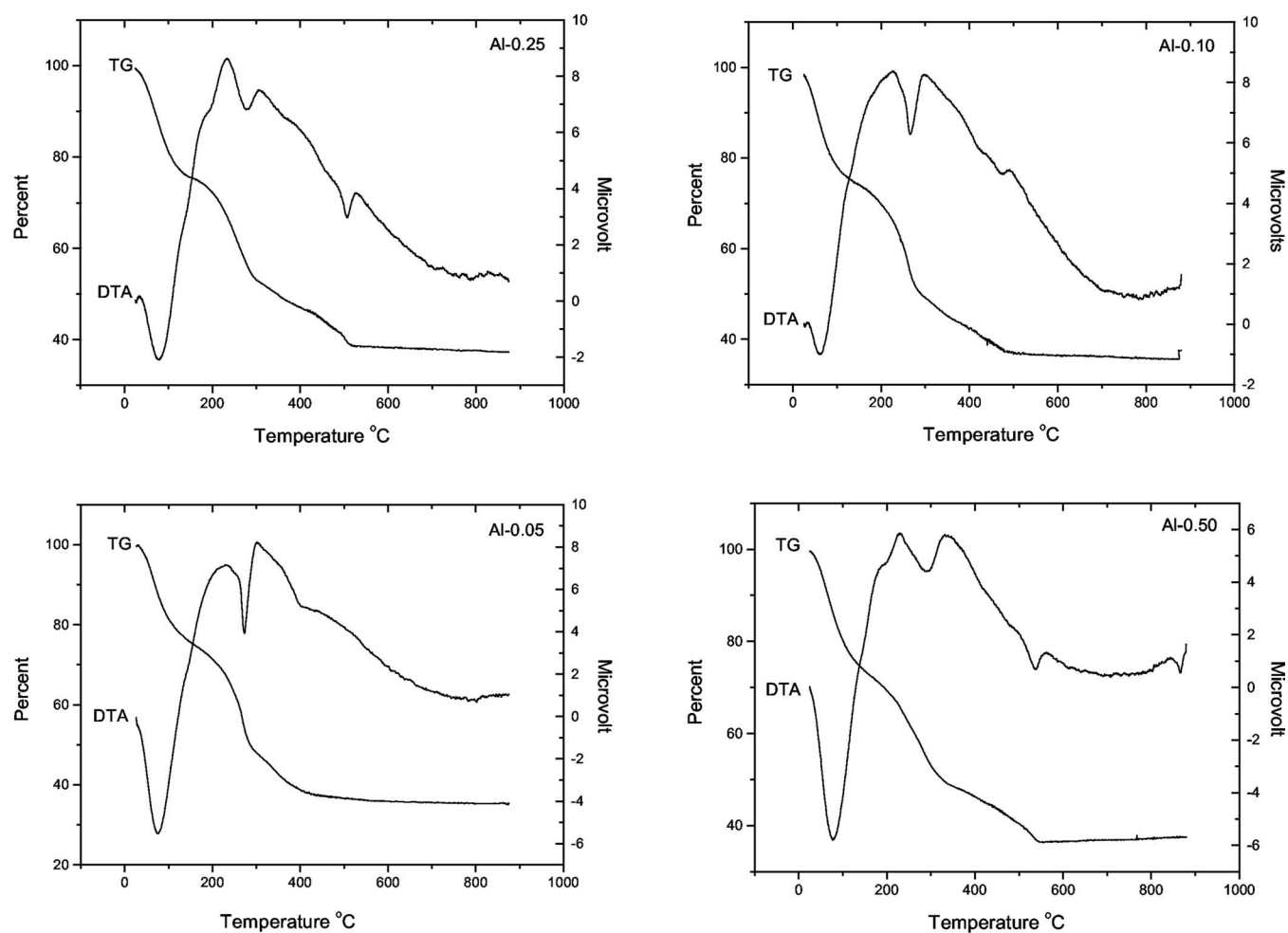


Figure 4. TG and DTA curves of  $\text{LiAl}_x\text{Ni}_{1-x}\text{VO}_4$  precursor.

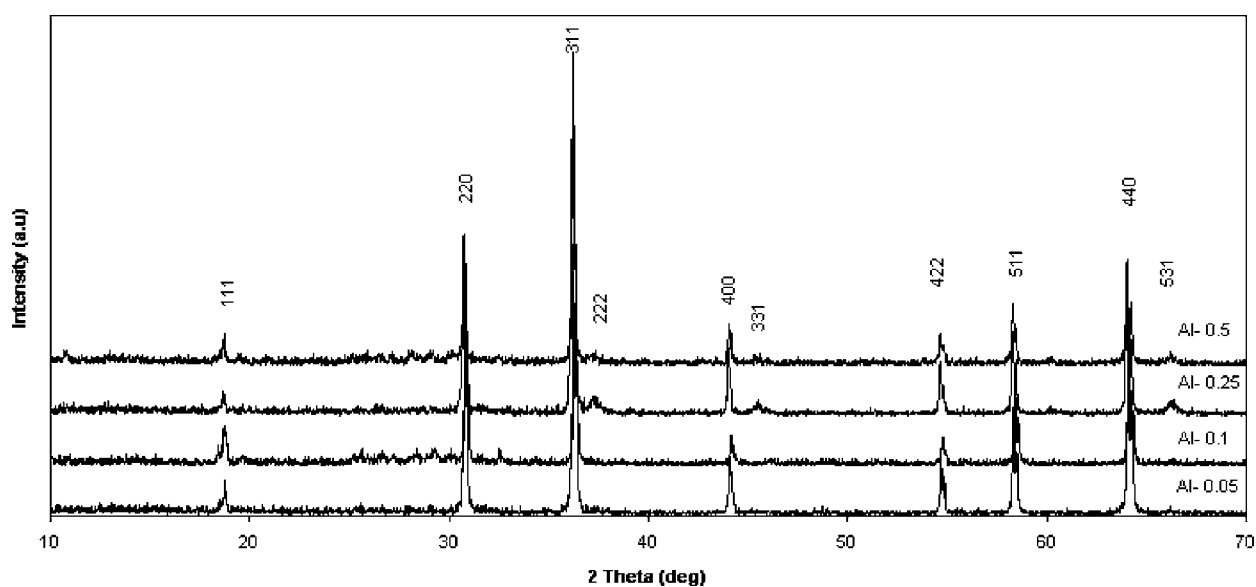


Figure 5. XRD patterns of the sol-gel-derived  $\text{LiAl}_x\text{Ni}_{1-x}\text{VO}_4$  powders calcined at 850°C.

**Table I. FTIR frequencies peaks observed for sol-gel synthesized LiNiVO<sub>4</sub>.**

No.	Temperature (°C)	Wavelength (cm <sup>-1</sup> )	Assignment
1	250	814.99	V—O bond of VO <sub>4</sub>
		951.89	VO <sub>4</sub> tetrahedron
		731.52	Li—O—Ni stretching
		644.38	Li—O stretching
2	450	815.99	V—O bond of VO <sub>4</sub>
		955.28	VO <sub>4</sub> tetrahedron
		731.83	Li—O—Ni stretching
		646.90	Li—O stretching
3	650	878.33	V—O bond of VO <sub>4</sub>
		947.34	VO <sub>4</sub> tetrahedron
		727.36	Li—O—Ni stretching
4	850	938.47	VO <sub>4</sub> tetrahedron

**FTIR spectroscopy.**— The FTIR spectra of LiNiVO<sub>4</sub> calcined at different temperatures (250, 450, 650, and 850°C) were recorded and the absorption peaks of the various stretching and bending vibrations are listed in Table I. The peaks for V=O and Ni—O are around 951.89 and 814.99 cm<sup>-1</sup>, respectively. The bands between 900 and 600 cm<sup>-1</sup> are associated with the stretching vibrations of V—O bonds of VO<sub>4</sub> tetrahedra in LiNiVO<sub>4</sub>.<sup>13-15</sup> Some evidence for the presence of a little residual carbonyl and nitrate moieties (450–525 cm<sup>-1</sup>) in the product at low calcination temperature are also reflected in the spectrum. As the calcination temperature is increased, the absorption peaks of the carbonyl group slowly vanish, leaving only the absorption bands of the V—O bonds.<sup>16</sup> This indicates the complete decomposition of the precursors and the formation of pure, single-phase LiNiVO<sub>4</sub>. Richardson and Ross<sup>17</sup> reported that the FTIR peaks for LiNiVO<sub>4</sub> were similar to those of a related compound LiMnVO<sub>4</sub> and those of the orthorhombic C<sub>m</sub>C<sub>m</sub>-type CrVO<sub>4</sub>. Touboul and Toledano<sup>18</sup> and Lytle<sup>19</sup> reported that the spinel-

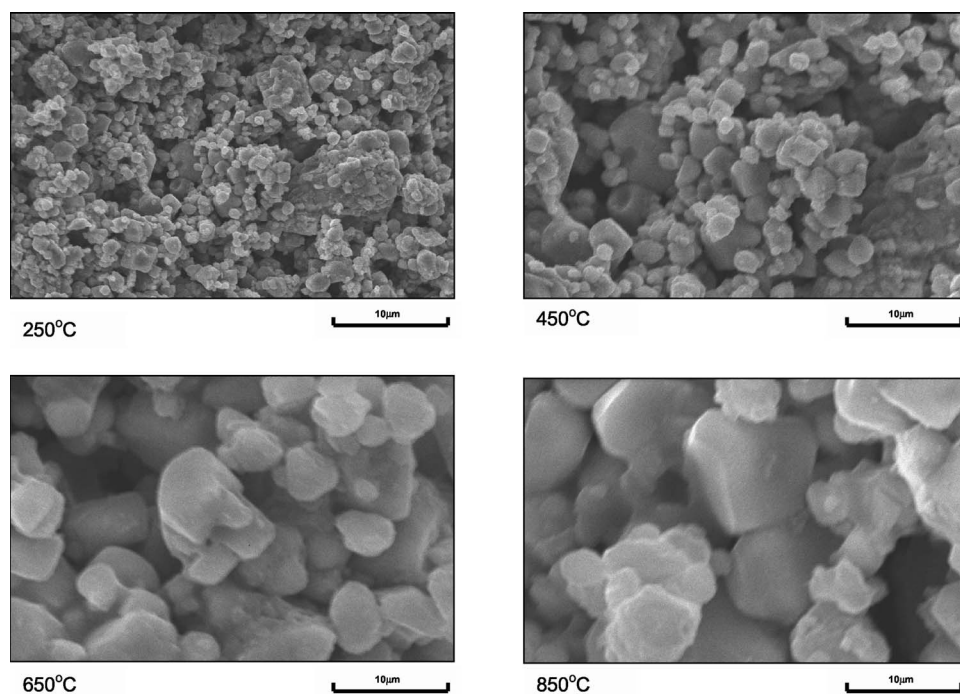
**Table II. FTIR frequencies peaks observed for sol-gel synthesized LiAl<sub>x</sub>Ni<sub>1-x</sub>VO<sub>4</sub>.**

No.	Temperature (°C)	Wavelength (cm <sup>-1</sup> )	Assignment
1	250	500	Li—O—Al stretching
		650	Li—O stretching
		725	Li—O—Ni stretching
		896	V—O bond of VO <sub>4</sub>
		915	VO <sub>4</sub> tetrahedron
2	450	950	Al—O—Ni stretching
		500	Li—O—Al stretching
3	650	650	Li—O stretching
		725	Li—O—Ni stretching
		897	V—O bond of VO <sub>4</sub>
		918	VO <sub>4</sub> tetrahedron
		950	Al—O—Ni stretching
4	850	897	V—O bond of VO <sub>4</sub>
		917	VO <sub>4</sub> tetrahedron
		950	Al—O—Ni stretching

related LiMnVO<sub>4</sub> compound would have [MnO<sub>6</sub>] octahedra where cation distributed LiVO<sub>4</sub> and VO<sub>4</sub> tetrahedra, which may neutralize the corners of tetrahedra with octahedral MnO<sub>6</sub>.<sup>15</sup>

FTIR spectra of LiAl<sub>x</sub>Ni<sub>1-x</sub>VO<sub>4</sub> at different temperatures, viz., 250, 450, 650, and 850°C, were recorded and the absorption peaks of the various stretching and bending vibrations are listed in Table II. The peaks for Li—O—Al, V—O, Ni—O, and Li—O are seen between 500 and 918 cm<sup>-1</sup>. The disappearance of the peaks between 450 and 525 cm<sup>-1</sup> in the samples calcined at 650 and 850°C are due to decomposition of carbonate salt of aluminum at higher temperature.

**SEM analysis.**— The electrochemical activity of cathode materials is influenced by the surface morphology of the particles. SEM images of the LiNiVO<sub>4</sub> inverse spinel calcined at different tempera-

**Figure 6.** SEM images of LiNiVO<sub>4</sub> particles calcined at different temperatures.

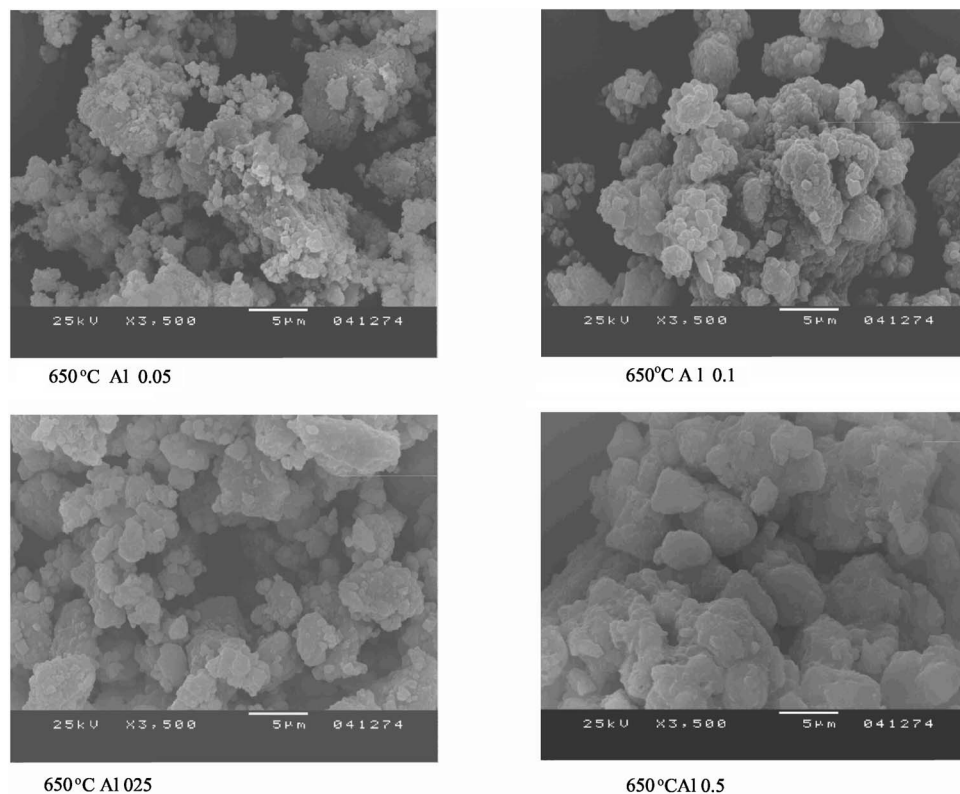


Figure 7. SEM images of different dopant level of  $\text{LiAl}_x\text{Ni}_{1-x}\text{VO}_4$  particles calcined at  $650^\circ\text{C}$ .

tures are depicted in Fig. 6. It is evident that the particles of the product obtained by calcination at  $250^\circ\text{C}$  are of micrometer-sized spherical grains. In fact, the products obtained by calcination at  $250$  and  $450^\circ\text{C}$  are agglomerates of finer particles. In general, good agglomeration and interparticle contact is useful in enhancing electrochemical activity. The samples calcined at  $650$  and  $850^\circ\text{C}$  had an ice-cube-like morphology. Further, a growth in the particle size is

apparent with increasing calcination temperature. The SEM images of  $\text{LiNiVO}_4$  calcined at  $450$ ,  $650$ , and  $850^\circ\text{C}$  show particles of size around  $1.0$ ,  $1.5$ , and  $2.5 \mu\text{m}$ , respectively.

Figure 7 shows the SEM pictures of  $\text{LiNiVO}_4$  with different levels of aluminum calcined at  $250^\circ\text{C}$ . It is evident that the surface morphology of the doped samples is similar to that of undoped samples at  $250^\circ\text{C}$ . However, a reduction in the particle size is observed at lower dopant levels. The growth in the particle size is seen as the aluminum content is increased.

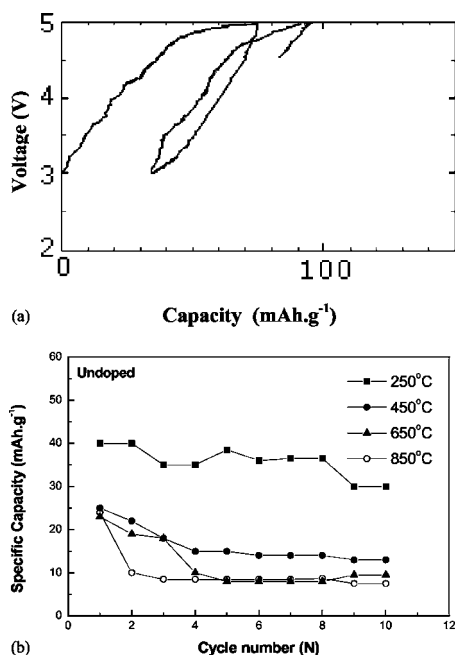


Figure 8. (a) Typical charge-discharge behavior of  $\text{LiNiVO}_4$  calcined at  $250^\circ\text{C}$ . (b) Cycle number vs capacity behavior of  $\text{LiNiVO}_4$  calcined at different temperatures.

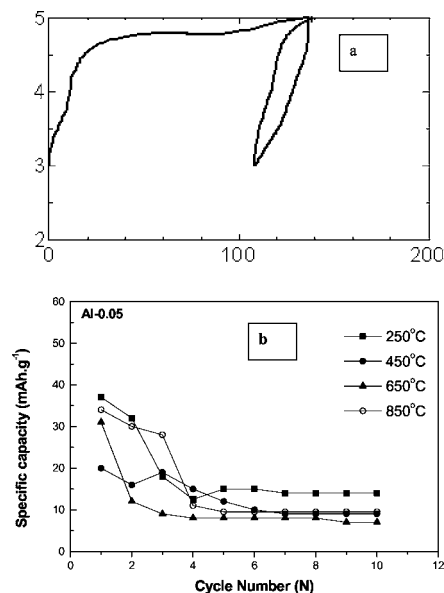
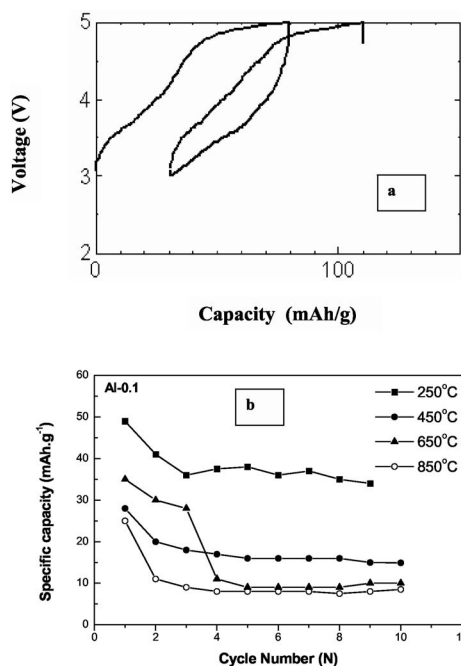
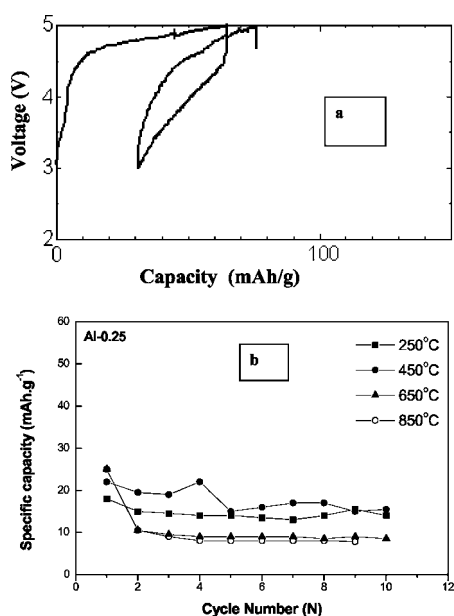


Figure 9. (a) Typical charge-discharge behavior of  $\text{LiAl}_{0.05}\text{Ni}_{0.95}\text{VO}_4$  calcined at  $250^\circ\text{C}$ . (b) Cycle number vs capacity behavior of  $\text{LiAl}_{0.05}\text{Ni}_{0.95}\text{VO}_4$  calcined at different temperatures.



**Figure 10.** (a) Typical charge–discharge behavior of  $\text{LiAl}_{0.10}\text{Ni}_{0.90}\text{VO}_4$  calcined at  $250^\circ\text{C}$ . (b) Cycle number vs capacity behavior of  $\text{LiAl}_{0.10}\text{Ni}_{0.90}\text{VO}_4$  calcined at different temperatures.

*Charge–discharge studies.*—Typical charge–discharge characteristics of  $\text{LiNiVO}_4$  calcined at  $250^\circ\text{C}$  and the cycling performance of  $\text{LiNiVO}_4$  calcined at different temperatures, viz., 250, 450, 650, and  $850^\circ\text{C}$ , are presented in Fig. 8a and b, respectively. It can be seen that undoped  $\text{LiNiVO}_4$  calcined at  $250^\circ\text{C}$  delivers  $40 \text{ mAh g}^{-1}$  during the first cycle and stabilizes at around  $35 \text{ mAh g}^{-1}$ . Samples calcined at higher temperatures show a negative trend in discharge capacity. After a few cycles, the capacity of the compound gradually decreases. Hence, it can be concluded that calcination at  $250^\circ\text{C}$  in



**Figure 11.** (a) Typical charge–discharge behavior of  $\text{LiAl}_{0.25}\text{Ni}_{0.75}\text{VO}_4$  calcined at  $250^\circ\text{C}$ . (b) Cycle number vs capacity behavior of  $\text{LiAl}_{0.25}\text{Ni}_{0.75}\text{VO}_4$  calcined at different temperatures.

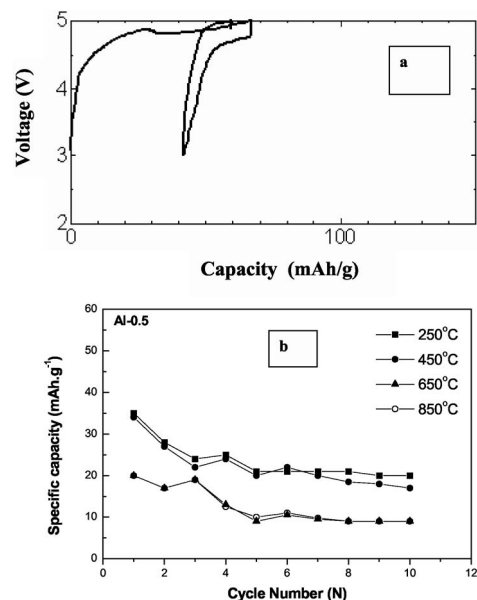


**Figure 12.** (a) Typical charge–discharge behavior of  $\text{LiAl}_{0.50}\text{Ni}_{0.50}\text{VO}_4$  calcined at  $250^\circ\text{C}$ . (b) Cycle number vs capacity behavior of  $\text{LiAl}_{0.50}\text{Ni}_{0.50}\text{VO}_4$  calcined at different temperatures.

the case of  $\text{LiNiVO}_4$  has better electrochemical activity compared to that obtained from the compounds synthesized at higher temperature.

Al-doped  $\text{LiNiVO}_4$  samples were prepared with different concentrations, viz., 0.05, 0.10, 0.25, and 0.50, and calcined at different temperatures, viz., 250, 450, 650, and  $850^\circ\text{C}$ . It was observed that the discharge capacity decreases with an increase in calcination temperature, irrespective of the dopant concentration. The calcination temperature of  $250^\circ\text{C}$  is quite satisfactory for better performance. These observations are in good agreement with that of pristine  $\text{LiNiVO}_4$ . Typical charge–discharge behavior and the cycling performance of  $\text{LiAl}_x\text{Ni}_{1-x}\text{VO}_4$  ( $x = 0.05, 0.10, 0.25, \text{ and } 0.50$ ) calcined at  $250^\circ\text{C}$  are presented in Fig. 9–12. Cycling studies of these materials indicate that the  $\text{LiAl}_{0.1}\text{Ni}_{0.9}\text{VO}_4$  sample calcined at  $250^\circ\text{C}$  shows better performance. Further,  $\text{LiAl}_{0.1}\text{Ni}_{0.9}\text{VO}_4$  exhibits a stable discharge capacity of  $35 \text{ mAh g}^{-1}$  over the investigated ten cycles. These results are superior to the earlier studies reported by Prabarhan et al.<sup>10</sup> involving a low-temperature synthesis and characterization of  $\text{LiNiVO}_4$  for Li-ion batteries. Further, Chitra et al.<sup>20</sup> reported that calcination of  $\text{LiNiVO}_4$  at  $800^\circ\text{C}$  delivers a discharge capacity of  $90 \text{ mAh/g}$  in the 1st cycle vs the theoretical value of  $148 \text{ mAh g}^{-1}$ . However, after five cycles the capacity dropped to  $15 \text{ mAh g}^{-1}$ , which was claimed to be superior to the result obtained by Fey and Wu.<sup>8</sup> A comparison of these results with our present studies indicate that the results obtained by us are superior, i.e., the undoped sample calcined at  $250^\circ\text{C}$  exhibits higher capacity retention of  $30 \text{ mAh g}^{-1}$ , even up to ten cycles. Further, all the samples calcined at higher temperature ( $850^\circ\text{C}$ ) suffer with severe capacity fade upon cycling. Thus, it is evident that calcination at higher temperature beyond  $250^\circ\text{C}$  for the synthesis of  $\text{LiNiVO}_4$  results in severe capacity loss upon cycling. It is seen from the discharge curves (Fig. 8–12) that the discharge capacities of Al-doped vanadate are slightly higher than that of pristine  $\text{LiNiVO}_4$ . It is interesting to note from Fig. 10b that the first discharge capacity of  $\text{LiAl}_{0.1}\text{Ni}_{0.9}\text{VO}_4$  calcined at  $250^\circ\text{C}$  is around  $50 \text{ mAh g}^{-1}$  resulting in a coulombic efficiency of 80%. However, upon cycling the discharge capacity of  $\text{LiAl}_{0.1}\text{Ni}_{0.9}\text{VO}_4$  stabilizes at around  $35 \text{ mAh g}^{-1}$ , corresponding to a coulombic efficiency of 60%. The coulombic efficiency was calculated using the ratio between the stable capacity of  $35 \text{ mAh g}^{-1}$  and the first charge capacity. Further, with increasing aluminum con-

tent beyond 0.1, poor discharge capacities result. This may be due to the tendency of Al-doped samples toward structural transformation from truly inverse spinel-to-spinel structure, as observed in the XRD pattern (Fig. 5). Thus, low levels of aluminum doping coupled with low-temperature calcination results in enhanced electrochemical performance of  $\text{LiNiVO}_4$ . Finally, it can be said that aluminum appears in the  $3^+$  valency state, replacing nickel ions in  $\text{LiAl}_x\text{Ni}_{1-x}\text{VO}_4$ , thereby changing oxidation state of vanadium from  $5^+$  to  $4^+$ , equivalent to the amount of aluminum added. Thus, it is expected that the plateau of vanadium oxidation from  $4^+$  to  $5^+$  could appear in the first discharge curve and this plateau should vanish with increasing aluminum content. This tendency is observed in the case of  $\text{LiAl}_{0.05}\text{Ni}_{0.95}\text{VO}_4$  and  $\text{LiAl}_{0.1}\text{Ni}_{0.90}\text{VO}_4$ , but the plateau rapidly decreases at higher aluminum content, viz., 0.25 and 0.5. This behavior could probably be attributed to the change in structure from inverse spinel to spinel structure.

### Conclusions

High-purity, micrometer-sized, monophasic  $\text{LiNiVO}_4$  particles have been successfully synthesized by a glycine-assisted sol-gel combustion method at temperatures as low as  $250^\circ\text{C}$  as confirmed by XRD and FTIR spectral studies. SEM images of the product show agglomerates of crystals of cubic morphology. It is demonstrated that the sol-gel combustion method can greatly lower the formation temperature. A low amount of aluminum and a low calcination temperature is found to be beneficial for enhanced electrochemical performance of  $\text{LiNiVO}_4$ . The discharge capacity and cycling performance of the  $\text{LiAl}_{0.1}\text{Ni}_{0.9}\text{VO}_4$  are superior at a calcination temperature of  $250^\circ\text{C}$ .

### Acknowledgment

This work was supported by the CREST program of Japan Science and Technology Agency, Tokyo, Japan.

Central Electrochemical Research Institute assisted in meeting the publication costs of this article.

### References

1. J. C. Bernier, P. Poix, and A. Michel, *Compt. Rend. Acad. Sci. (Paris)*, **253**, 1578 (1961).
2. G. T. K. Fey, W. Li, and J. R. Dahn, *J. Electrochem. Soc.*, **141**, 2279 (1994).
3. G. T. K. Fey, J. R. Dahn, M. J. Zhang, and W. Li, *J. Power Sources*, **68**, 549 (1997).
4. G. T. K. Fey, *J. Active Passive Electron. Compon.*, **18**, 110 (1995).
5. G. T. K. Fey and W. B. Perng, *Mater. Chem. Phys.*, **47**, 279 (1997).
6. G. T. K. Fey, K. S. Wang, and S. M. Yang, *J. Power Sources*, **68**, 159 (1997).
7. G. T. K. Fey, J. R. Dahn, M. J. Zhang, and W. Li, Extended Abstracts of the 8th Int. Meeting on Lithium Batteries, Boston, MA, p. 426 (1996).
8. G. T. K. Fey and C. S. Wu, *J. Pure Appl. Chem.*, **69**, 2329 (1997).
9. Y. Ito, *Tech.*, **11**, 11 (1986).
10. R. S. Prabaharan, M. S. Michel, S. Radhakrishna, and C. Julien, *J. Mater. Chem.*, **7**, 1791 (1997).
11. R. Kanno, Y. Kawamoto, Y. Takeda, M. Jasegwa, O. Yamamoto, and N. Kinomusa, *J. Solid State Chem.*, **96**, 397 (1992).
12. M. J. Isasi, R. Saez-puche, M. L. Vegia, C. Piem, and A. Jerez, *Mater. Res. Bull.*, **23**, 595 (1998).
13. M. Sato, S. Kano, S. Tamak, M. Misawa, Y. Shirakawa, and M. Ohashi, *J. Mater. Chem.*, **6**, 1191 (1996).
14. J. Preudhomme and P. Tarte, *Spectrochim. Acta, Part A*, **28**, 69 (1972).
15. N. Kalaiselvi, A. Ganesh Kumar, C. Sathyakumar, V. R. P. Gokul, T. Thangaraj, N. G. Renganathan, and N. Muniyandi, *Portu. Electrochim. Acta*, **20**, 89 (2002).
16. J. R. Liu, M. Wang, X. Lin, D. C. Yin, and W. D. Huang, *J. Power Sources*, **108**, 113 (2002).
17. T. J. Richardson and P. N. Ross, *Mater. Res. Bull.*, **31**, 935 (1995).
18. M. Toubol and P. Toledano, *Acta Crystallogr., Sect. B: Struct. Crystallogr. Cryst. Chem.*, **B36**, 240 (1980).
19. F. W. Lytle, *Acta Crystallogr., Sect. A: Cryst. Phys., Diffraction, Theor. Gen. Crystallogr.*, **A22**, 32 (1967).
20. S. Chitra, P. Kalyani, B. Yebka, T. Mohan, E. Haro-Poniatowski, R. Gangadharan, and C. Julien, *Mater. Chem. Phys.*, **65**, 32 (2000).